Localized pulsed nanosecond discharges in a counterflow nonpremixed flame environment

2015 Plasma Sources Sci. Technol. 24 055010

(http://iopscience.iop.org/0963-0252/24/5/055010)

IOP Publishing Plasma Sources Science and Technology

Plasma Sources Sci. Technol. **24** (2015) 055010 (10pp) doi:10.1088/0963-0252/24/5/055010

Localized pulsed nanosecond discharges in a counterflow nonpremixed flame environment

C Guerra-Garcia[1], M Martinez-Sanchez[1], R B Miles[2] and A Starikovskiy[2]

[1] Department of Aeronautics and Astronautics, Massachusetts Institute of Technology, Cambridge, MA 02139, USA
[2] Department of Mechanical and Aerospace Engineering, Princeton University, Princeton, NJ 08544, USA

E-mail: cguerrag@mit.edu

Received 13 March 2015, revised 19 July 2015
Accepted for publication 6 August 2015
Published 27 August 2015

Abstract

A flame is a very unusual environment for the development of a gas discharge, since it presents strong gradients in temperature, composition, and pre-ionization. In this paper we examine how such an environment impacts the development of the plasma when using repetitive pulsed nanosecond discharges, one of the main strategies used in the field of plasma assisted combustion. Experiments were performed in a counterflow nonpremixed burner with parallel electrodes at the nozzle exits and nanosecond-resolved photography of the plasma emission is presented. It was shown that the discharge development in stratified media may take place in the form of a dielectric barrier discharge with a localized energy deposition. In the experiments presented the discharge energy was coupled to the flame front because of the high rate of chemi-ionization and the gas density decrease in the flame.

Keywords: pulsed nanosecond discharge, counterflow nonpremixed flame, *in situ* energy deposition

(Some figures may appear in colour only in the online journal)

1. Introduction

Non-thermal plasmas can assist flames in numerous ways [1, 2]. They can participate in the inflammation process [3], speeding it up [4, 5]. They can be used to mitigate thermo-acoustic instabilities, facilitating the use of otherwise unstable ultra-lean flames [6]. More generally, plasmas can extend lean flammability limits [7], blow-out limits [8], increase flame speeds [9], and enable a more complete combustion [10].

The possibilities for impacting a flame with a plasma, through the additional chemistry it introduces [11–13], are varied; an important choice being where to position the plasma source relative to the flame. From this standpoint, two possibilities have been explored: producing the plasma upstream of the flame, or overlapping plasma and flame.

In the first case, previous research has shown that the energy is transferred through a combination of thermal and non-thermal effects. In general, it is not easy to deliver very reactive species created by the plasma to the flame front when they are generated away from it due to their short lives. For example, a high *E/n* discharge in oxygen produces atomic oxygen in $O(^3P)$, $O(^1D)$, $O(^1S)$ states, ions O_2^+ and O^+, free electrons, excited molecular oxygen in $O_2(a^1\Delta_g)$ and $O_2(b^1\Sigma_g^+)$ states and ozone O_3. From these species, ozone and the excited molecular oxygen are the most stable species, and all other species are quenched much faster. E.g. at 300 K and atmospheric pressure, electron ion recombination for a concentration of electrons of $n_e \sim 10^{13}$ cm^{-3} through $O_2^+ + e^- \rightarrow O(^3P) + O(^1D)$ takes ~0.5 μs [1]; quenching of the $O(^1D)$ state through the process $O(^1D) + O_2 \rightarrow O(^3P) + O_2$ occurs in ~1 ns [14]; and $O(^3P)$ recombines through $O(^3P) + O_2 + O_2 \rightarrow O_3 + O_2$ in ~1 μs [14]. Therefore, effective transport of these shorter life species can only be ensured either through an accompanying temperature increase or

through the creation of more stable intermediate species [9]. The temperature increase is due to a rapid heating of the gas, which depends primarily on the reduced electric field. For electric fields ~100 Td, the main source (~10–15% of the total deposited energy) has been explained as self-quenching reactions of excited nitrogen $N_2(A^3\Sigma_u^+)$ [15, 16].

More specifically, when the non-thermal plasma is created in the *oxidizer stream*, the main energy paths that produce flame enhancement are the excitation of molecular oxygen to $O_2(a^1\Delta_g)$ and $O_2(b^1\Sigma_g^+)$ [9, 17], and the creation of ozone [18]. If the oxidizer is air, NO_x will also be generated and is a well-known promoter for oxidation reactions [19]. The role of the excited molecular oxygen is to reduce the activation barrier of O, H and OH formation; and the impact of ozone addition is that it acts as a cold transport means of O by attachment to O_2. Eventually, these two energy paths intensify the chain reactions at the reaction front by an enhanced production of radicals. The relevance of the direct production of O atoms was evaluated by [20], who concluded that, in order for the discharge-produced O atoms to reach the reaction zone, the oxidizer temperature needed to increase above a certain threshold to avoid recombination of the atomic oxygen.

On the other hand, for a plasma produced in the *fuel stream*, the main kinetic path that is being activated is cracking of the large fuel molecules into smaller fragments, large unsaturated or branched hydrocarbons, and H_2 [10, 21]. Similarly, when the plasma is produced in a *premixed reactant stream*, the main effect is to pre-oxidize the fuel with the subsequent heat release [22] and partial fuel conversion into H_2, CO [8, 23], alcohols, aldehydes and peroxides [1].

A different story arises when the plasma is produced close enough to the reaction zone, a strategy known as *in situ energy deposition*. Recently, [24] showed that by overlapping a repetitively pulsed nanosecond discharge to a counterflow nonpremixed flame, atomic oxygen created by the discharge could directly participate in the combustion reactions. In this case, the discharge was not localized to the flame front but rather acted uniformly on the fuel and oxidizer regions as well as in the reaction zone. Better coupling of the plasma energy to the flame has been achieved using microwave (MW) energy [25–27] and femto-second lasers [28]. In these cases, the plasma energy deposition was fully superimposed to the flame front. The coupling of the MW energy to the flame front was proposed to be through direct electron heating whereas, when using femto-second lasers, radicals (O atoms and hydrocarbon radicals) were thought to be readily created. An ultimate way of directly coupling the external energy to the flame was proposed by the authors of [29], who used a laser to draw a pre-ionization pattern for the discharge propagation and then increased the energy deposition using MW. All in all, a clear advantage of these different localized energy deposition strategies is that the energy is spatially coupled to a specific region of interest, and contact with possible electrodes, that can erode or even melt, is avoided.

In this paper we explore another strategy to localize the plasma energy at the location of the flame, this time using high-voltage ns-duration discharges. It is here proposed that the unusual environment for plasma development encountered in a flame field, characterized by sharp gradients in composition, temperature and pre-ionization, can be exploited to achieve a selective breakdown of the flame alone by use of a fast modulated electric discharge.

2. Selective electrical breakdown of a region of favorable ionization

In [30], it was demonstrated that when using repetitive pulsed nanosecond discharges a selective breakdown of a region of favorable ionization could be obtained, without bridging the inter-electrode space or even without contact with the electrodes. The idea proposed was that layers of gas with very different ionization properties could be arranged in such a way as to create a dielectric barrier discharge (DBD)-type behavior, in which the role of the dielectric barrier was played by the most insulating gas [31].

In [30], the hypothesis was demonstrated using a layered gas structure with a layer of helium sandwiched between two nitrogen layers, and the parameters were chosen to have selective breakdown of the helium zone, while the nitrogen layers remained non-conductive. This was possible thanks to the very different ionization coefficients of helium and nitrogen. More specifically, the ionization coefficient α, or electron production per unit length, is given by Townsend's semi-empirical formula:

$$\frac{\alpha}{n} = F_i \exp\left(-\frac{G_i}{E/n}\right), \tag{1}$$

where F_i and G_i are constants that depend on the composition, n is the local number density of the gas, and E/n is the local reduced electric field. In particular $G_{He} \ll G_{N_2}$. A detailed model was proposed to predict the different breakdown modes that could appear in such a configuration, which for fixed parameters and gradually increasing applied voltage were: no breakdown, breakdown of the helium layer alone and breakdown of the full gap. In essence the model only depended on a few parameters, mainly: the composition of the gases present, the temperature ratio of the layers, the ratio of thicknesses of the layers, the applied voltage, and the classical nd_h parameter (where d_h is the thickness of the easier to ionize layer).

When thinking about a nonpremixed flame, it can be very crudely described as a layer of heated gas (at the peak flame temperature) surrounded by colder gas (at the reactants temperature) so that a similar situation can, in principle, take place. In this case, the main enhancement factor of the ionization coefficient in the flame with respect to the surrounding gas is the intensification of the reduced electric field through the gas density decrease with the temperature increase at constant pressure conditions ($E/n \sim T$). The experiments described in what follows aim to explore this effect.

3. Experimental setup

The test bed of choice to assess the feasibility of directly coupling a ns-duration plasma to a flame is the laminar

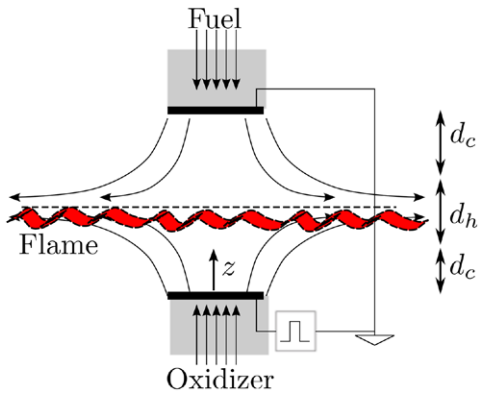

Figure 1. The counterflow nonpremixed flame. Two parallel electrodes are placed at the nozzle exits. d_h refers to the thickness of the high temperature region, and d_c to the thickness of the lower temperature reactant flows.

counterflow nonpremixed flame with two parallel mesh electrodes placed at the exit of the burner nozzles (figure 1).

This setup has two clear advantages. First, the applied electric field is aligned with the direction of variation of the gas properties and the platform is essentially one-dimensional. Second, the applied electric field is close to uniform so that the dominant gradients are due to the presence of the flame and differences in the jets, and not to the particular electrode geometry.

3.1. Counterflow burner

The nonpremixed flame experiments were performed in a counterflow burner that consisted on two concentric quartz nozzles with inner diameter of 15 mm. The fuel was injected from the top nozzle and the oxidizer from the bottom nozzle. Both flows were surrounded by a co-flow ring of inner diameter 18 mm and outer diameter 22 mm through which nitrogen was injected to quench the periphery of the flame, provide isolation from the environment and reduce flame curvature. The tubes were separated by $L = 17$ mm. Quartz was used to provide electrical insulation and avoid unwanted discharges. A schematic of the setup is shown in figure 2.

The bottom nozzle was placed on a two-axis translation stage, in the plane parallel to the nozzle exit, and with control over the inclination of this plane for precise positioning of both nozzles relative to each other.

The fuel, oxidizer and dilutant flows in the inner tubes were supplied via upstream sonic nozzles from compressed gas bottles and the flow rate was varied using the upstream pressure. For the co-flows, the flow rate was measured using variable area flowmeters and varied using needle valves. Glass beads and ceramic honeycomb were inserted in the tubes as flow straighteners and turbulence suppression elements.

For the results in section 4.1, the top quartz tube had a silicon carbide heater (SER Starbar) inserted in it and was insulated with a ceramic blanket.

The exit velocities of the jets were chosen to be momentum-balanced, in order to have the stagnation plane for the colliding flows, and the flame, sitting close to the center of the burner

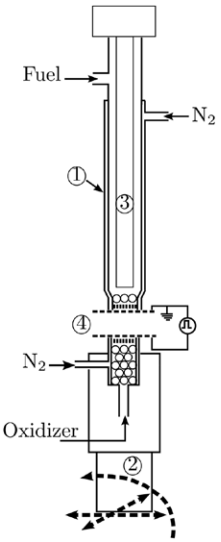

Figure 2. Counterflow burner setup. (1) Concentric quartz tubes; (2) translation stages; (3) heater; (4) discharge cell.

gap. The velocities of the co-flows were chosen to be approximately the same as those of the respective main flows.

The flames considered were methane-air flames and, for the fuel jet, different degrees of dilution in nitrogen were tested (see figure 3). All experiments were performed at atmospheric pressure. Further details of the setup can be found in [32].

3.2. Discharge cell

Two stainless-steel square meshes of 50 mm width were placed at the exit of the nozzles to serve as electrodes. Accurate positioning of the electrodes relative to each other was achieved using alumina spacers. The capacitance of the discharge cell was measured to be 2.3 pF (maximum stored energy, for voltage pulses of 15 kV, of ~260 μJ pulse^{-1}). The electrodes were directly connected to the power supply through a 15 m coaxial cable (RG 302/U) with an impedance of 75 Ω.

The top mesh was grounded and the bottom mesh was powered using a high voltage pulse generator (FID Technologies FPG 10–30NKS10). The voltage pulses were unipolar (positive), had a maximum amplitude ranging from 2 to 10 kV into a 100–500 Ω load, rise time of 2 ns and duration of around 10 ns at 90% of maximum voltage. The repetition frequency could be varied in the range 2–30 kHz. A typical voltage pulse waveform (as measured at the discharge cell) for the experiments performed is shown in figure 4.

The electrical properties of the discharge were monitored using a high voltage probe (LeCroy PPE 20 kV) and a current probe (Pearson 2877) coupled to a 20 dB attenuator (Agilent 8493A-20). Both voltage and current were measured by an Agilent oscilloscope (1 GHz Infiniium 54835A).

3.3. Ns-resolved photography

To resolve the plasma dynamics of the nanosecond-duration discharge coupled to a flame, a PicoStar HR12 (LaVision GmbX) intensified charge-coupled device (ICCD) camera was

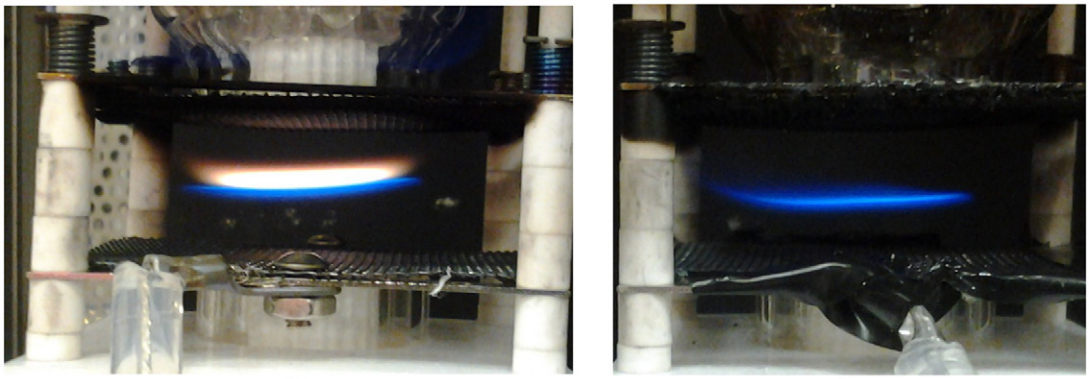

Figure 3. Representative photographs of the baseline flames (the oxidizer is air in both cases). $X_{CH_4,f}$ is the mole fraction of methane in the fuel jet. (a) Pure methane, $X_{CH_4,f} = 1$. (b) Methane diluted in nitrogen, $X_{CH_4,f} = 0.19$.

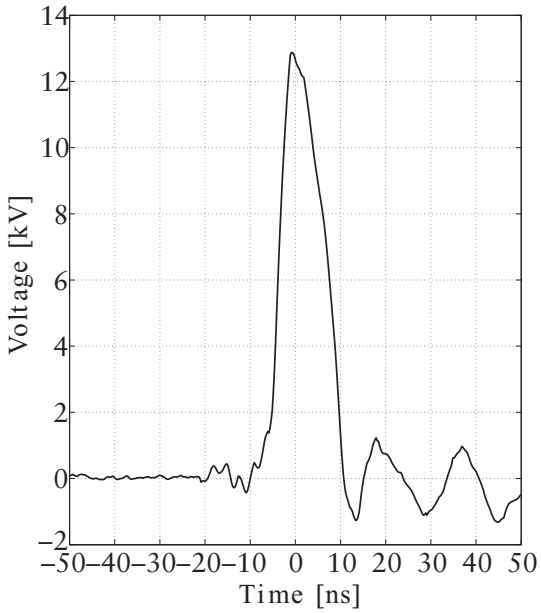

Figure 4. Representative voltage waveform of repetitive nanosecond high-voltage pulses.

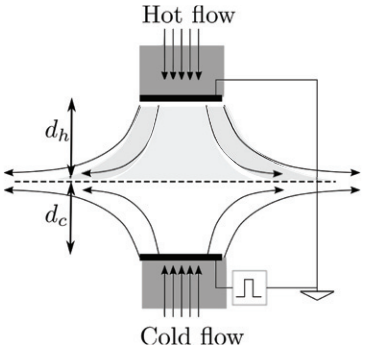

Figure 5. Schematic of the discharge development in a stratified gas flow.

used. The timing between the image intensifier, the electronic shutter and the high voltage pulse generator was controlled with a delay generator (BNC Model 575). The images taken correspond to the integrated emission over a broad wavelength range. Different delays of the camera were introduced with respect to the application of the voltage pulse to obtain the discharge evolution in time. This time-resolved visualization assumes that the discharges are repeatable since the sequential images correspond to different applied voltage pulses. The camera gate used was 0.5 ns. Images were delayed by 1 ns between them.

4. Results

4.1. Selective excitation of a high temperature/low density region

A preliminary experiment was performed to verify the hypothesis that high temperature regions in a flow can be ionized selectively when applying ns-duration pulses. For this purpose, ns-pulses were applied across non-isothermal flow using the same opposed jets platform described in section 3.1. Helium was chosen as the working gas since the applied voltage required for breakdown is lower than for other gases (and compatible with the available equipment). The configuration of the setup used in this experiment is shown in figure 5.

Helium was injected from both nozzles. The top jet was heated to 900 K and the bottom jet was at ambient temperature. The opposed jets were momentum balanced so that the stagnation plane lay in the middle of the gap, and $d_h \approx d_c$ (see figure 5). The exit velocity of the cold jet was 2.5 m s^{-1}. For this experiment, no nitrogen co-flow was used.

Ns-pulses of variable amplitude at frequency $f = 3$ kHz were applied to the bottom mesh, the top mesh was grounded. The applied voltage was gradually increased to observe the transition from a fully confined plasma to the heated region to full breakdown of the gap.

Digital camera photographs of this experiment are shown in figure 6. Figure 6(a) demonstrates the confinement of the plasma emission to the heated jet when applying ns-pulses of 7.4 kV amplitude (all quoted voltage levels are as measured at the discharge cell). The plasma emission extended to the approximate position of the stagnation plane.

By increasing the applied voltage, all other parameters fixed, the emission suddenly bridged the full gap although the two regions, of the *hot* and *cold* jets, could still be clearly identified due to the stronger emission from the hot jet. A

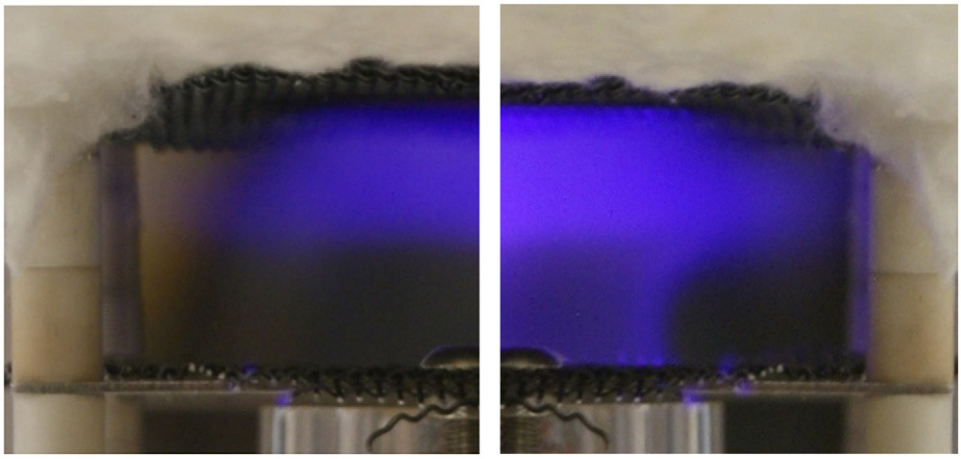

Figure 6. Effect of increasing the applied voltage for ns-pulses in a stratified flow. Only half of the domain is shown to highlight the transition of breakdown modes with the applied voltage increase. At the lower voltage ($V_p = 7.4$ kV) selective excitation of the high temperature (low density) region is observed, whereas for the higher voltage ($V_p = 12$ kV) there is full breakdown of the gap. The exposure time of the camera is 1/6 s, corresponding to the accumulation of 500 voltage pulses. (a) $V_p = 7.4$ kV. (b) $V_p = 12$ kV.

representative image of full-breakdown is shown in figure 6(b) for an applied volage of 12 kV. If the voltage was decreased to the initial value, confinement to the *hot* jet was recovered.

In all cases, the discharge observed had a diffuse and uniform glow-like appearance. The plasma emission was confined to the helium jets, and the limiting streamlines (between the helium opposed jets and the ambient air) could be sharply identified visually, due to the very different ionization properties of the helium jets as compared to ambient air.

The results can be explained as follows. For low enough applied voltages, the breakdown threshold can be locally met within the high temperature jet while ionization cannot proceed in the low temperature jet. I.e. for a reduced electric field of 53 Td (7.4 kV over the 17 mm gap at 900 K and atmospheric pressure), and using the ionization parameters for helium $F_{He} = 9.32 \cdot 10^{-21}$ m^2 and $G_{He} = 105$ Td [33], the product $\alpha_h d_h$ is close to 90, so that Meek's criterion is met [33] (the subscript h refers to the heated jet). For the low-temperature jet the E/n value is 18 Td and $\alpha_c d_c$ is too small for discharge development (the subscript c refers to the cold jet).

Once charged species are created in the hot layer it becomes partially conductive and the electric field across it decreases. When this happens, the electric field in the cold layer increases (since the voltage across the discharge gap remains the same) and avoidance of breakdown needs to be ensured accounting for this enhancement after plasma creation in the hot jet.

In conclusion, the images presented confirm that pulsed nanosecond discharges can be confined to regions of favorable ionization due to a local increase in the reduced electric field through its temperature dependence. The electrons created in the *hot* jet are free to drift towards the anode but their energy is too low to produce any further ionization and excitation in the *cold* region (or at least ionization and excitation are greatly reduced). As the voltage is increased, the breakdown threshold is reached in the cold jet and the transition to breakdown of the full gap can take place.

4.2. Plasma coupling to a flame

In terms of its electrical properties, the structure of the counterflow nonpremixed flame is partly similar to the configurations of section 4.1 and [30]: it consists on a high temperature layer surrounded by gas at a much lower temperature and higher density. For this configuration, the peak flame temperature and the thickness of the flame can be modified by the degree of dilution of the reactant flows and the strain rate, and the ionization coefficients F and G depend on the composition.

More specifically, the flame thickness is inversely proportional to the square root of the product of pressure and strain rate, so that the ratio of the thickness of the high temperature region of the flame, d_h, to the thickness of the lower temperature reactant zones, d_c, scales as (see diagram in figure 1):

$$\frac{d_h}{d_c} = 2\left(\frac{L}{d_{h,\mathrm{ref}}}\sqrt{\frac{\mathrm{ap}}{a_{\mathrm{ref}}p_{\mathrm{ref}}}} - 1\right)^{-1}, \qquad (2)$$

where L is the distance between nozzles, p is the pressure, a the strain rate, and the subscript 'ref' refers to some reference quantities.

In this section, the fuel is pure methane, the oxidizer is air, the experiment is performed at atmospheric pressure, and the strain rate is 25 s^{-1}. For these conditions, the ratio of the peak temperature of the flame to the ambient temperature is estimated as $T_{max}/T_{amb} \approx 6.8$ and the geometrical factor as $d_h/d_c \approx 0.9$. Using these parameters and the simplified estimation of [30], an applied voltage of ~15 kV should enable a selective breakdown of the flame high temperature region without exciting the reactant jets.

Figure 7 shows representative sequential images of the emission evolution during application of the 1000th pulse in a train. With the exposure time used, the emission corresponds almost exclusively to transitions of the second positive system

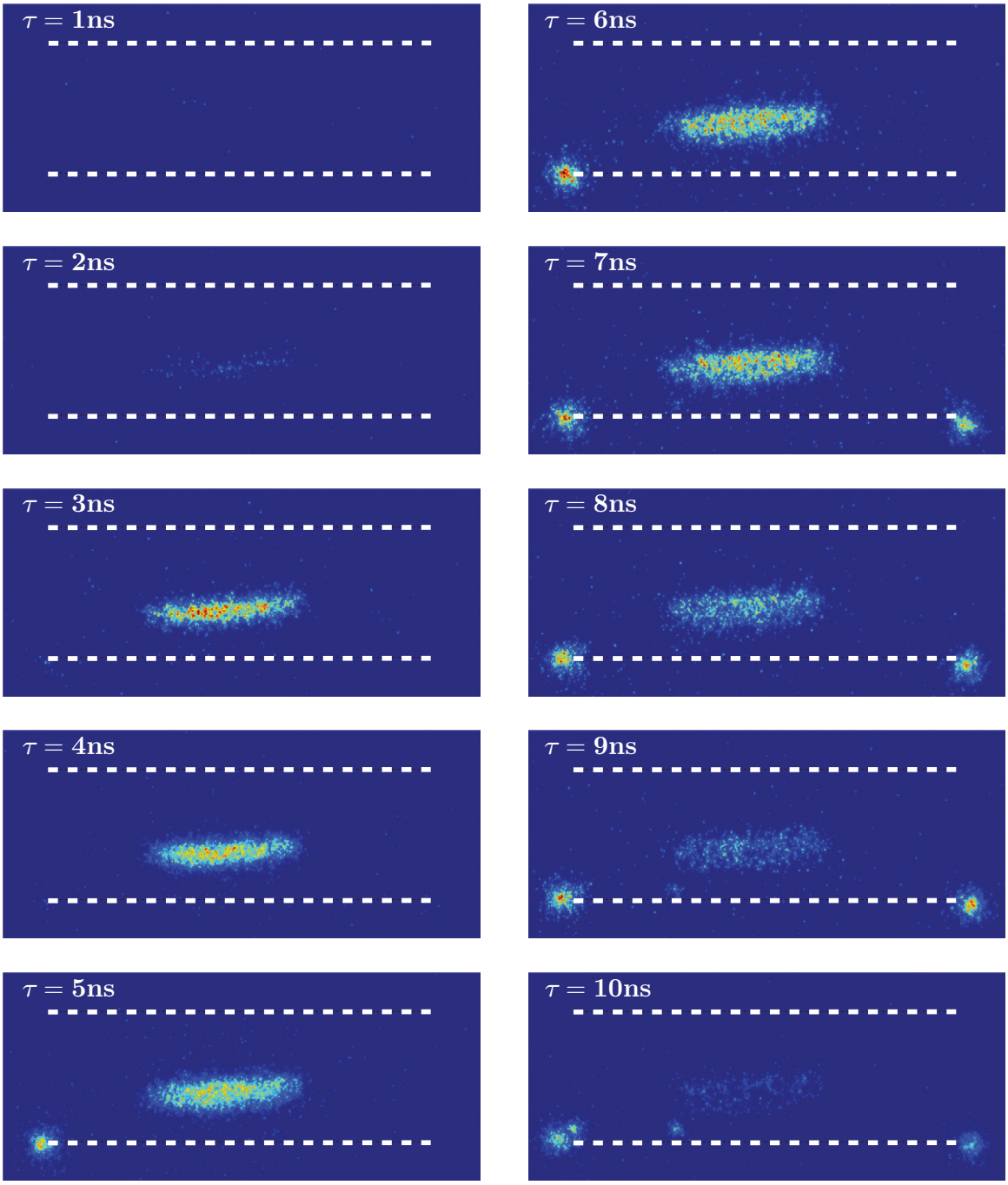

Figure 7. Time evolution of the plasma emission coupled to the flame. Images correspond to sequential photographs during pulse number 1000 in a train. The exposure time is 0.5 ns. The electrodes' positions are marked by the white lines. The elongated ellipsoidal emission corresponds to plasma coupled to flame; the smaller circular emission regions are an experimental artifact as a result of using square electrodes with sharp edges.

of molecular nitrogen. Note that, without voltage pulse application, no light is captured by the camera, even in the presence of the flame, so that the emission corresponds to the plasma excitation alone. The localization of the discharge to the regions of high temperature, high E/n, is clear in these images: the emission comes from either the flame region (low n) or from the sharp edges of the square electrodes (high E). Indeed, when applying voltage pulses of $\sim$15.5 kV amplitude, 20 ns duration, and at a repetition rate of 25 kHz, the excitation created by the ns-pulses was confined to the flame region alone.

It must be clarified that although the flame power is $\sim$65 W and the maximum electrical power that could be delivered to the flame at 25 kHz is $\sim$6.5 W, or 10% of flame power, the actual power that was coupled to the flame was $<$1% since the inter-electrode gap was not bridged by the conductive path [34].

Tests with lower pulse repetition frequencies also led to the localization, but a frequency of 25 kHz was selected for illustrative purposes. For the frequencies accessible with the power supply, the applied pulses should behave almost

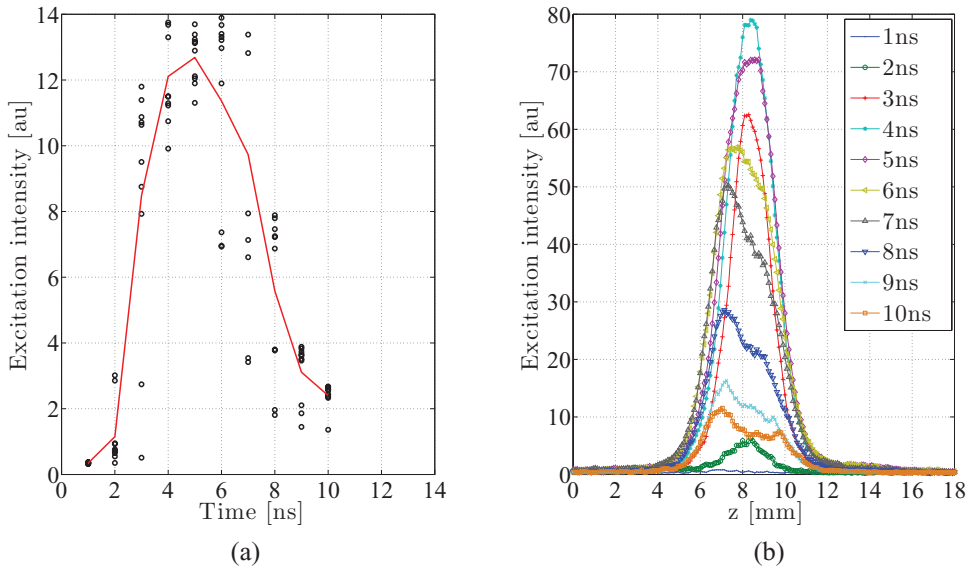

Figure 8. Time evolution of the integrated plasma emission and spatial profiles across the flame (pulse number 1000). z is measured from the anode (bottom nozzle), as defined in figure 1. The black circles in (a) correspond to individual photographs and the continuous red line is the averaging across all images taken. (a) Time evolution. (b) Spatial profile.

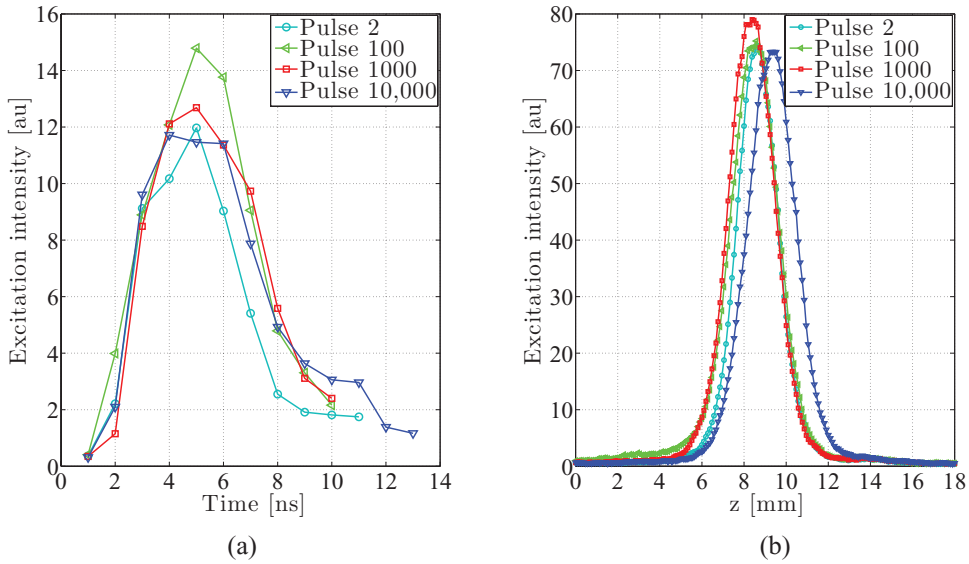

Figure 9. Time evolution of the integrated plasma emission and spatial profiles across the flame (pulse numbers 2, 100, 1000 and 10 000). z is measured from the anode (bottom nozzle), as defined in figure 1. (a) Time evolution. (b) Spatial profile at peak emission, 4 ns.

Table 1. Measured FWHM of plasma emission.

Pulse number	FWHM [mm]
2	2.2
100	2.6
1000	2.6
10 000	2.7

independently as the typical recombination time for $n_e \sim 10^{12}$ –10^{13} cm^{-3} is on the order of a few microseconds (using the dissociative recombination rate of [35]), as compared to the time between pulses of 40 μs. In addition, the role of cumulative heating is minimal due to the low energy release.

Photographs of the evolution of the plasma, during application of a voltage pulse, were taken with an exposure time of 0.5 ns and a delay between images of 1 ns to record the emission evolution in space and time at the timescale relevant to the plasma emission (section 3.3). The mean of 10 images was used in the results presented in figures 8 and 9.

From these images, the evolution in time of the integrated emission of a region 9.5 mm along the center of the flame and 17 mm across the flame, is shown in figure 8(a). The black circles correspond to the 10 individual photographs taken and the continuous red line is the average value across those images. The emission lasts for ~10 ns, consistent with the time of the discharge development. This time is shorter than the high-voltage pulse and indicates the time of low-density region ionization and electric field redistribution in the gap. It should be noted that the collisional quenching of the $N_2(C^3\Pi_u)$ state at atmospheric pressure conditions is an extremely fast process:

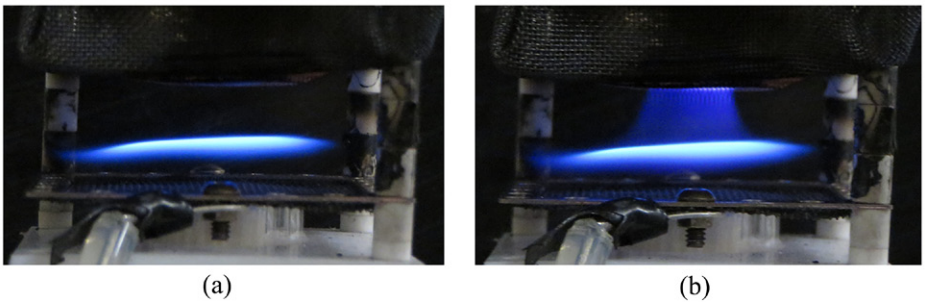

Figure 10. Selective ns-duration high-voltage excitation of the fuel jet by choice of dilutants. Top jet (fuel) is diluted in helium, bottom jet (oxidizer) is diluted in nitrogen. (a) Baseline flame. (b) Discharge coupled to fuel jet.

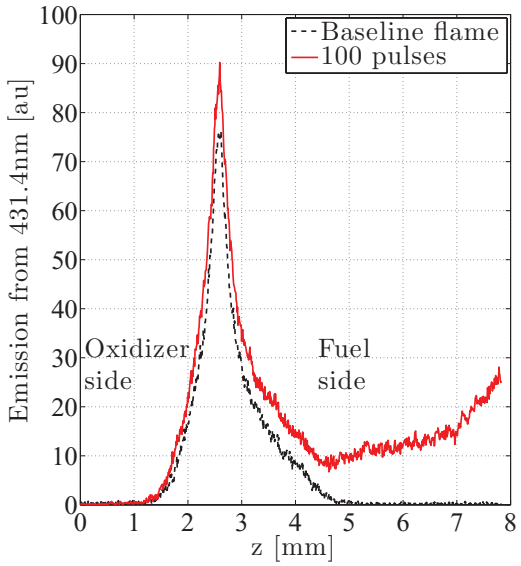

Figure 11. Spatially resolved emission from CH^* at 431.4 nm, case of selective ns-duration high-voltage excitation of the fuel jet by choice of dilutants. z is measured from the anode (bottom nozzle), in this case, the origin of the measurement is arbitrary.

using the deactivation rate constant of $N_2(C^3\Pi_u, \nu = 0)$ by O_2 given in [36], the quenching time of $N_2(C^3\Pi_u, \nu = 0)$ in atmospheric pressure air at ambient temperature is ~0.7 ns. That is why the emission in nanosecond time scale reflects mainly the rate of C^3 state population by electron impact.

The evolution in time of the emission profiles *across* the flame are shown in figure 8(b). The localization of the profiles is evident: except for a region ~6 mm wide, there is no emission. The discharge develops during a few nanoseconds (the emission reaches the maximal value between the 2nd–4th nanosecond after the discharge start). After this point the redistribution of the electric field leads to a significant decrease of the excitation rate and emission of the nitrogen second positive system (figure 8(b)). The electrical field decreases in the conductive flame zone and increases in cold parts of the flow. The bottom surface of the flame located at 6 mm above the anode, becomes a virtual cathode for the new discharge gap 0–6 mm. Figure 8(b) demonstrates the higher emission from this virtual cathode layer at the time 6–10 ns after the discharge start. This effect explains the asymmetry of the emission profile during the late phases of the discharge development.

The experiment was repeated for pulses number 2, 100, 1000 and 10 000 in a train. Figure 9 compares the evolution in time of the integrated emission and of the emission profiles across the flame (at peak emission) for the different pulses. The profiles are very similar in all cases, indicating that all the pulses have an equivalent impact on the gas. Note that no firm conclusions should be derived from the slight shift of the profile of pulse 10 000 with respect to the other pulses since slight regulations were made during the experiment to the flow of the nitrogen shroud. Table 1 summarizes the full width at half maximum (FWHM) of the emission at 4 ns. The emission profile width increases from pulse number 2 to pulse number 100 because of the formation of a steady-state pre-ionization distribution, and remains constant after this point.

A final comment must be made related to the, globally, very-fuel rich flame used in this experiment. In this case the fuel jet was pure methane, leading to a sooty flame (figure 3(a)), and prompting the doubt of whether there could be a possible reinforcement due to the presence of soot particles. This point was addressed by checking the strategy with non-sooty, highly diluted flames, for which the same coupling was visually observed.

5. Further discussion

5.1. Chemi-ionization electrons

For completeness of the discussion, it must be recognized that, aside from the composition and temperature gradients accounted for, there is an additional factor that affects the electrical energy coupling, arising from the natural pre-ionization present at the flame front. Even before applying an electric field above the breakdown threshold, ions and electrons are generated within the high-temperature zones of hydrocarbon flames in amounts much in excess of thermodynamic equilibrium values [37]. This excess ionization is due to chemi-ionization reactions, the most important reaction being:

$$CH + O \longrightarrow CHO^+ + e^-, \qquad (3)$$

where the CH is either in ground state or electronically excited [38]. Since the CH radicals are only present in the reaction zone of hydrocarbon flames, that is where high populations of charged species are encountered [39]; e.g. the FWHM of the electron density profile has been reported to be $\delta_i \sim 0.6$ mm, for a stoichiometric premixed methane-air flame [40, 41]. Note that this thickness may vary with the flame parameters but, in

general, will be of the order of a fraction of a mm, which is much less than the thickness of the high temperature region: $\delta_i < d_h$. The chemi-ionization fraction of a flame depends primarily on the equivalence ratio and ranges from $n_i/n \approx 10^{-8}$ –10^{-7}, where the peak is encountered at stoichiometric conditions [42]. This pre-existing ionization will impact the way the electrical energy is coupled to the gas [27, 41, 43, 44].

In particular, when using pulsed discharges, these electrons serve as an initial seeding for the development of the electron avalanches upon application of a high-voltage pulse. Note that the high density plasma seed is encountered precisely within the high temperature region, exacerbating the differences between the *cold* and *hot* regions of the gas and contributing to the localization of the discharge. These seed electrons can also facilitate the sustained operation of the discharge by providing a minimum population of electrons at all times, since normally the repetitive pulsed discharge strategy relies on the use of high frequency to maintain this baseline level [34, 45]. Indeed, if the chemi-ionization electron density is higher than the minimum electron density between two consecutive voltage pulses (due to the recombination of the discharge-produced electrons), then the seed electrons available for the upcoming pulse will be the chemi-ionization electrons, and so a single pulse would behave similarly to continuous pulses. This was observed in the experiments by the very similar emission profiles for pulses number 2, 100, 1000, and 10 000 in a train. Finally, this pre-ionization also contributes to the homogeneity of the discharge: for a high number of simultaneous primary avalanches adjacent avalanches will overlap, smoothing out the local gradients [46, 47].

5.2. Versatility of the coupling

As a final comment, the discussion can be extended to include other excitation modes; determined by the composition, the geometry of the burner, the pressure and the strain rate. As an illustrative example, by choosing gases with very different electrical properties for the oxidizer and fuel jets, the excitation can be favored in either. This can be done by diluting the methane and the oxygen in different inert gases. E.g. for a fuel jet of (CH_4:He = 0.125:0.875) and an oxidizer jet of (O_2: N_2 = 0.41:0.59) at a strain rate of 40 s^{-1}, selective excitation of the fuel jet is possible, as shown in figure 10. In this case, the voltage pulses had 15.5 kV amplitude and a repetition frequency f = 25 kHz.

Figure 11 shows the spatially resolved, across the flame, emission around the 431.4 nm peak of the CH band without applied pulses and after the accumulation of 100 ns-pulses (integrated emission in 4 ms). The peak of excited CH marks the position of the flame front. When applying the high voltage ns-pulses strategy, the fuel is *activated*, shown by the presence of excited CH out of the flame front region.

6. Conclusion

The experiments reported have confirmed that gas excitation by high voltage ns-duration pulses can be fully coupled to the flame region, demonstrating that selective excitation of the flame and *in situ* plasma coupling is possible when using pulsed voltage within a wide range of parameters. In this case, the selective plasma energy deposition is possible due to a combination of the medium stratification and the presence of chemi-ionization electrons. Note that the laminar counterflow flame platform can be used as a building block for the more readily encountered turbulent nonpremixed flame. Therefore, these results offer a partial image of the energy coupling in a complex combustion situation with flamelets and hot spots.

Future work should address the impact this localized plasma strategy can have on the flame as well as the kinetics of the coupling.

Acknowledgments

C Guerra wants to acknowledge funding of her work through an MIT Aero-Astro Vos' fellowship, as well as an Amelia Earhart scholarship to support her visit to Princeton University. The work was partially supported by Air Force Office of Scientific Research in the framework of the project 'Fundamental Mechanisms, Predictive Modeling and Novel Aerospace Applications of Plasma Assisted Combustion'.

References

[1] Starikovskiy A and Aleksandrov N 2013 *Prog. Energy Combust. Sci.* **39** 61–110
[2] Starikovskaia S M 2014 *J. Phys. D: Appl. Phys.* **47** 353001
[3] Kosarev I N, Khorunzhenko V I, Mintoussov E I, Sagulenko P N, Popov N A and Starikovskaia S M 2012 *Plasma Sources Sci. Technol.* **21** 045012
[4] Pancheshnyi S V, Lacoste D A, Bourdon A and Laux C O 2006 *IEEE Trans. Plasma Sci.* **34** 2478–87
[5] Do H, Cappelli M A and Mungal M G 2010 *Combust. Flame* **157** 1783–94
[6] Moeck J P, Lacoste D A, Laux C O and Paschereit C O 2013 *51st AIAA Meeting including the New Horizons Forum and Aerospace Exposition* (*Grapevine, Texas*) pp 2013–0565
[7] Pilla G, Galley D, Lacoste D A, Lacas F, Veynante D and Laux C O 2006 *IEEE Trans. Plasma Sci.* **34** 2471–7
[8] Kim W, Mungal M G and Cappelli M A 2008 *Appl. Phys. Lett.* **92** 051503
[9] Ombrello T, Won S H, Ju Y and Williams S 2010 *Combust. Flame* **157** 1916–28
[10] Rosocha L A, Coates D M, Platts D and Stange S 2004 *Phys. Plasmas* **11** 2950–6
[11] Bozhenkov S A, Starikovskaia S M and Starikovskii A Y 2003 *Combust. Flame* **133** 133–46
[12] Kosarev I N, Aleksandrov N L, Kindysheva S V, Starikovskaia S M and Starikovskii A Y 2009 *Combust. Flame* **156** 221–33
[13] Aleksandrov N L, Kindysheva S V, Kosarev I N, Starikovskaia S M and Starikovskii A Y 2009 *Proc. Combust. Inst.* **32** 205–12
[14] Atkinson R, Baulch D L, Cox R A, Hampson R F Jr., Kerr J A, Rossi M J and Troe J 1997 *J. Phys. Chem. Ref. Data* **26** 1329–499
[15] Aleksandrov N L, Kindysheva S V, Nudnova M M and Starikovskiy A Y 2010 *J. Phys. D: Appl. Phys.* **43** 255201
[16] Popov N A 2001 *Plasma Phys. Rep.* **27** 886–96

[17] Starik A M, Kozlov V E and Titova N S 2008 *J. Phys. D: Appl. Phys.* **41** 125206
[18] Ombrello T, Won S H, Ju Y and Williams S 2010 *Combust. Flame* **157** 1906–15
[19] Ombrello T, Ju Y and Fridman A 2008 *AIAA J.* **46** 2424–33
[20] Sun W, Uddi M, Ombrello T, Won S H, Carter C and Ju Y 2011 *Proc. Combust. Inst.* **33** 3211–8
[21] Stange S, Kim Y, Ferreri V, Rosocha L A and Coates D M 2005 *IEEE Trans. Plasma Sci.* **33** 316–7
[22] Sun W, Uddi M, Won S H, Ombrello T, Carter C and Ju Y 2012 *Combust. Flame* **159** 221–9
[23] Kim W, Do H, Mungal M G and Cappelli M A 2008 *IEEE Trans. Plasma Sci.* **36** 2898–904
[24] Sun W, Won S H, Ombrello T, Carter C and Ju Y 2013 *Proc. Combust. Inst.* **34** 847–55
[25] Shinohara K, Takada N and Sasaki K 2009 *J. Phys. D: Appl. Phys.* **42** 182008
[26] Stockman E S, Zaidi S H, Miles R B, Carter C D and Ryan M D 2009 *Combust. Flame* **156** 1453–61
[27] Michael J B, Chng T L and Miles R B 2013 *Combust. Flame* **160** 796–807
[28] Yu X, Peng J, Yang P, Sun R, Yi Y, Zhao Y, Chen D and Yu J 2010 *Appl. Phys. Lett.* **97** 011503
[29] Michael J B 2012 *PhD Thesis* Princeton University
[30] Guerra-Garcia C and Martinez-Sanchez M 2013 *J. Phys. D: Appl. Phys.* **46** 345204
[31] Guerra-Garcia C and Martinez-Sanchez M 2015 *Appl. Phys. Lett.* **106** 041601
[32] Guerra-Garcia C 2014 *PhD Thesis* Massachusetts Institute of Technology
[33] Raitzer Y 1991 *Gas Discharge Physics* (Berlin: Springer-Verlag)
[34] Pai D, Stancu G D, Lacoste D A and Laux C O 2009 *Plasma Sources Sci. Technol.* **18** 045030
[35] Packan D 2003 Repetitive nanosecond glow discharge in atmospheric pressure air *PhD Thesis* Stanford University
[36] Pancheshnyi S V, Starikovskaia S M and Starikovskii A Y 2000 *Chem. Phys.* **262** 349–57
[37] Lawton J and Weinberg F J 1964 *Proc. R. Soc.* A **277** 468–97
[38] Cool T A and Tjossem P J H 1984 *Chem. Phys. Lett.* **111** 82–8
[39] Semenov E S and Sokolik A S 1970 Combustion, explosion and shock waves *Fiz. Goren. Vzryva* **6** 33–43
[40] MacLatchy C S 1979 *Combust. Flame* **36** 171–8
[41] Ju Y, Macheret S O, Shneider M N and Miles R B 2004 *40th AIAA Joint Propulsion Conf. and Exhibit (Fort Hauderdale, FL)* 2004–3713
[42] Calcote H F 1961 *Symp. Int. Combust.* **8** 184–99
[43] Sullivan D J, Zaidi S H, Macheret S O, Ju Y and Miles R B 2004 *40th AIAA Joint Propulsion Conf. and Exhibit (Fort Hauderdale, FL)* 2004–3713
[44] Stockman E M 2009 *PhD Thesis* Princeton University
[45] Pai D 2008 *PhD Thesis* École Centrale Paris
[46] Palmer A J 1974 *Appl. Phys. Lett.* **25** 138–40
[47] Levatter J I and Lin S 1980 *J. Appl. Phys.* **51** 210–22